Original

Razzaq, M.Y.; Behl, M.; Lendlein, A.:
Memory-effects of magnetic nanocomposites
In: Nanoscale (2015) Royal Society of Chemistry

DOI: 10.1039/c2nr31332d

Nanoscale

Cite this: *Nanoscale*, 2012, **4**, 6181

www.rsc.org/nanoscale

FEATURE ARTICLE

Memory-effects of magnetic nanocomposites

Muhammad Yasar Razzaq, Marc Behl and Andreas Lendlein*

Received 29th May 2012, Accepted 30th July 2012
DOI: 10.1039/c2nr31332d

The thermally induced shape memory effect (SME) is the capability of a material to fix a temporary (deformed) shape and recover a 'memorized' permanent shape in response to heat. SMEs in polymers have enabled a variety of applications including deployable space structures, biomedical devices, adaptive optical devices, smart dry adhesives and fasteners. By the incorporation of magnetic nanoparticles (mNP) into shape-memory polymer (SMP), a magnetically controlled SME has been realized. Magnetic actuation of nanocomposites enables remotely controlled devices based on SMP, which might be useful in medical technology, *e.g.* remotely controlled catheters or drug delivery systems. Here, an overview of the recent advances in the field of magnetic actuation of SMP is presented. Special emphasis is given on the magnetically controlled recovery of SMP with one switching temperature T_{sw} (dual-shape effect) or with two T_{sw}s (triple-shape effect). The use of magnetic field to change the apparent switching temperature ($T_{sw,app}$) of the dual or triple-shape nanocomposites is described. Finally, the capability of magnetic nanocomposites to remember the magnetic field strength (H) initially used to deform the sample (magnetic-memory effect) is addressed. The distinguished advantages of magnetic heating over conventional heating methods make these multifunctional nanocomposites attractive candidates for *in vivo* applications.

1 Introduction

SMP are materials which can be deformed and fixed in a temporary shape and from which they recover their original shape only when exposed to an appropriate stimulus such as heat or light.[1–5] The high technological importance of SMP became apparent in the 1960s when covalently crosslinked polyethylene found its way into heat shrinkable tubing and films, which are applied in packaging and mechatronics today. Significant efforts to study the SME in polymers began in the late 1980s and this trend was continuously intensified. Among the different classes of SMP the most extensively investigated group is thermally induced SMP, which are triggered by heat. Here, the SME is triggered once a certain switching temperature T_{sw} is exceeded. The shape-memory capability is not an intrinsic material property. It results from the combination of a suitable polymer

Center for Biomaterial Development, Institute of Polymer Research, Helmholtz-Zentrum Geesthacht, Kantstr. 55, 14513 Teltow, Germany. E-mail: andreas.lendlein@hzg.de

Muhammad Yasar Razzaq

Muhammad Yasar Razzaq is currently pursuing his doctoral degree under the supervision of Prof. Dr A. Lendlein. He obtained his masters in Chemistry from Quaid-i-Azam University, Islamabad. His current research activities focus on synthesis and investigation of organic–inorganic nanostructured materials with an emphasis on magneto-sensitive shape-memory polymers.

Marc Behl

Marc Behl received his diploma in Chemistry from the University of Wuppertal and his doctor's degree from the Johannes Gutenberg University, Mainz. Currently, he is the head of the Active Polymers Department at the Center for Biomaterial Development in the Institute of Polymer Research at the Helmholtz-Zentrum Geesthacht. His primary research interests are design, synthesis, and characterization of materials capable of active movement with a focus on shape-memory polymers.

architecture in addition to a tailored processing procedure, which is called programming or in particular "dual-shape creation procedure" (DSCP) to differentiate this programming from that of multiple shapes (see below).[6,7] The SME in SMP relies on the temporary fixation of oriented polymer chain segments, which recover their original shape upon stimulation due to entropy driven relaxation of the chain segments. Hence, suitable SMP provide a polymer network architecture, which consists of netpoints and molecular switches being sensitive to an external stimulus. The netpoints interconnect the chain segments and determine the permanent shape of the polymer. The netpoints can be either of chemical nature (covalent bonds) or of physical nature (intermolecular interactions). Chemically crosslinked SMP can be achieved through suitable crosslinking chemistry applied either by heat (thermosets) or light (photosets). SMP, in which the netpoints are provided by physical interaction, require a polymer morphology consisting of at least two segregated domains as found *e.g.* in block copolymers. Here the phase with the highest thermal transition (T_{perm}) is acting as the netpoint.[4,7] As the permanent shape is created by processing from the melt, these SMP are often referred to as thermoplastic SMP. The chain segments associated with the domains with the second highest thermal transition T_{trans} are acting as molecular switches and are therefore called switching domains.

During DSCP, the thermally induced SMP are heated above T_{trans} deformed in the viscoelastic state of the switching domains to an elongation ε_m by application of an external stress, and then cooled below the thermal transition temperature T_{trans} associated with the switching domains.

The solidification of switching domains forms additional crosslinks. These secondary crosslinks can rely on vitrification or crystallization of domains formed by side chains or the chain segments connecting two netpoints. Consequently, T_{trans} related to the molecular switch can be either a glass transition temperature (T_g) or a melting temperature (T_m). Only when these secondary crosslinks dominate the netpoints determining the permanent shape, they enable the temporary fixation of an elastic deformation, which can be recovered by reheating the programmed sample under constant strain or under stress-free conditions. In this way T_{sw} can be tuned by appropriate programming conditions.[8] The tensile stress σ as a function of temperature is determined in the recovery process under constant strain conditions, while under stress-free conditions the deformation ε as a function of temperature is measured. In addition, T_{sw} can be determined by the first derivation of stress *versus* temperature or as the temperature $T_{\sigma,max}$ at which maximum stress is developed from constant strain experiments. The cycle of DSCP and recovery can be repeated several times whereby the temporary shapes can be varied from one to the next cycle. The effect can be quantified by determining the shape-fixity ratio (R_f) and the shape-recovery ratio (R_r). R_f describes the ability of the switching segment to fix the mechanical deformation, which has been applied during the programming process. R_f is equal to the ratio of the strain in the stress-free state after the withdrawal of the tensile stress in the N^{th} cycle $\varepsilon_u(N)$ and the maximum strain ε_m.

$$R_f(N) = \frac{\varepsilon_u(N)}{\varepsilon_m} \quad (1)$$

The recovery of the original shape is quantified by R_r which indicates how well the original shape has been recovered. R_r can be calculated from $\varepsilon_u(N)$ and the extension at the tension-free states $\varepsilon_p(N-1)$ and $\varepsilon_p(N)$ while stretching the sample in two subsequent cycles $N-1$ and N.[3,4,9–14]

$$R_r(N) = \frac{\varepsilon_u(N) - \varepsilon_p(N)}{\varepsilon_u(N) - \varepsilon_p(N-1)} \quad (2)$$

In addition to these classical SMP, which are able to transform from a first (temporary) shape to a second (permanent) shape and are therefore referred to as dual-shape polymers (DSP), triple-shape polymers (TSP) or multiple-shape polymers (MSP) have been introduced recently. TSP and MSP are based on thermo-sensitive multiphase polymer network architectures (*e.g.* AB copolymer networks or grafted copolymer networks). When stimulated by two subsequent increases in environmental temperature, these TSP can perform more complex active movements by changing from a first shape A to a second shape B and from there to a third shape C.[1,15–20] On the molecular level, the triple-shape capability was realized by the incorporation of two switching segments into the polymer network, which provided at least two segregated domains resulting in two thermal transition temperatures $T_{trans,A}$ and $T_{trans,B}$. Covalent crosslinks, which were established during the polymer network formation, determined the original shape C, while additional physical crosslinks, which were created in a two-step thermomechanical programming process, fixed shapes A and B. The physical crosslinks providing shape B are associated with the highest transition temperature $T_{trans,B}$, while the second highest transition temperature $T_{trans,A}$ determines shape A. Both $T_{trans,B}$ and $T_{trans,A}$ can either be a T_m or T_g. The triple-shape effect (TSE) is created by the application of a two-step (TCP-2s) or single-step (TCP-1s) thermomechanical treatment called triple-shape creation procedure (TCP). The triple-shape capability of

Andreas Lendlein

Andreas Lendlein is Director of the Institute of Polymer Research at Helmholtz-Zentrum Geesthacht in Teltow, Germany and Member of the Board of Directors of the Berlin-Brandenburg Centre for Regenerative Therapies (BCRT). He is a professor at the University Potsdam and Honorary Professor at Freie Universität Berlin as well as Member of the Medical Faculty of Charité University Medicine Berlin. He completed his Habilitation in Macromolecular Chemistry in 2002 at RWTH Aachen University and received his doctoral degree in Materials Science from the Swiss Federal Institute of Technology (ETH) in Zürich in 1996. His current research interests include (multi)functional polymer-based materials, biomaterials and their interaction with biological environments as well as the development of medical devices and controlled drug delivery systems especially for regenerative therapies.

the material is characterized by the extent to which the subsequently memorized shapes B and C are recovered. These shape changes are quantified by the strain recovery rates R_r(A → B) and R_r(A → C), and two distinct T_{sw}s, T_{sw}(A → B) and T_{sw}(B → C), which can be determined as inflection points from the strain–temperature curve obtained under stress-free recovery.[15,16,19,21–24]

In polymers having high elasticity and a broad transition temperature (ΔT_g or ΔT_m) associated to the switching domains, the variation of the programming temperature T_{prog} at which the permanent shape is deformed for creating a shape-memory influenced the recovery kinetics[25,26] or the T_{sw},[27,28] at which the SME occurred. The latter effect was initially reported for polyvinyl alcohol–carbon nanotube nanocomposites, in which a linear correlation between T_{sw} and T_{prog} was found in the range of ΔT_g.[28] This ability to remember the temperature T_{prog}, where the polymer was deformed recently is named the temperature memory effect (TME). Recently, temperature-memory polymers (TMP) with crystallizable controlling units could be successfully created as well.[29] Here, the thermomechanical treatment, which was named the temperature-memory creation procedure (TMCP) was designed in such a way that the mechanical deformation ε_m is predominantly fixed by the volume fraction of the crystallites associated with a T_m close to T_{prog}. The fixation of the temporary, deformed shape is controlled by a tailored combination of thermally and strain-induced crystallization. T_{prog} was varied within ΔT_m of the crystallizable switching domains. After TMCP the recovery process was conducted under constant strain or stress-free conditions. During constant strain recovery, the maximum stress σ_{max} at a temperature $T_{\sigma,max}$ was determined, while for recovery under stress-free conditions T_{sw} was determined as the inflection point of the strain–temperature recovery curve. The variation of T_{prog} applied during TMCP enabled the adjustment of T_{sw} or $T_{\sigma,max}$ in polymers exhibiting a broad thermal transition (ΔT_g or ΔT_m).[29–31]

Besides triggering the SME by direct heating, indirect actuation by immersion in water or other solvents, *e.g.* *N*,*N*-dimethylformamide (DMF), has been demonstrated in commercially available SMP.[32–35] Here, the lowering of T_{trans} by diffusion of low molecular weight solvent molecules into the polymer bulk acting as a plasticizer triggers the SME, while the sample temperature remained constant.[34] However, the recovery time was much lower as compared to the direct heating method. For SMP intended for biomedical applications, body temperature is suggested as the activation temperature from the naturally regulated heat supply of the body. However, body temperature does not always allow the shape recovery to proceed in a well controlled way regarding the recovery magnitude and kinetics.[36,37] Therefore, alternative methods of heating inside the body including the use of lasers to heat a device at the location of implantation have been investigated. Lasers as a heating source feature a higher on-demand character for the activation of the SME compared to other conventional heating sources. In a laser-activated medical device based on shape-memory polyurethane (SMPU), the indirect actuation of SME was achieved for the mechanical removal of blood clots.[38,39] However, the use of a laser during the procedure required extra equipment and regulatory barriers attributed to the risk that potential overheating of the device could cause damage to the surrounding tissue.

An alternative to laser heating is the use of inductive heating to remotely actuate SMP. Inductive heating of SMP was achieved by the creation of magnetic nanoparticle composites (MNPC).[40–42] Magnetic nanoparticles (mNP) dissipate heat in an alternating magnetic field (AMF) through hysteresis losses and/or additional mechanisms based on different kinds and sizes of the particles and can be heated even at locations deep within the body. Various ferro- or ferrimagnetic nanoparticles, *e.g.* iron/iron oxide, nickel, or cobalt compounds have been used as fillers to develop MNPC.[43] Among these mNP, magnetite (Fe_3O_4) nanoparticles (MNP) are of special interest, especially for biomedical applications due to their high magnetization ability, low cytotoxicity, and high biocompatibility.[44–46] When a programmed SMP MNP composite (SMP-MNPC) was exposed to an AMF, the heat generated in the MNP spread into the polymer matrix and increased the sample temperature. As soon as the temperature exceeded T_{sw} of the SMP matrix, the recovery of the permanent shape could be observed.[36,47,48] A typical equipment suitable for the exploration of such a magnetically induced SME consists of a high-frequency generator, a water cooled coil and a temperature detector such as an IR pyrometer for non-contact measurement of the sample temperature (Fig. 1).[36]

Different methods used to incorporate MNP into SMP matrices include *ex situ* methods, *i.e.* dispersion of the synthesized nanoparticles into the polymeric solution,[49,50] or *in situ* monomer polymerization methods in the presence of the nanoparticles.[51] However, these methods suffer extremely from the high agglomeration tendency of the nanosized particles, as the nanoparticles tend to reduce their surface energy by aggregation. The aggregation of particles can result in sedimentation of these aggregates during nanocomposite formation, which act as defects and have detrimental effects on uniform heating of SMP-MNPC under AMF. During the synthesis, the expected composite viscosity determines the applied dispersing technology. Low viscous reactive resin based mixtures can be processed with mechanical stirrers or by sonication under ambient or slightly elevated temperatures. For highly viscous polymer matrices, processing techniques, *e.g.* a mixer–kneader or extrusion can be used. In the latter case, high shear forces depending

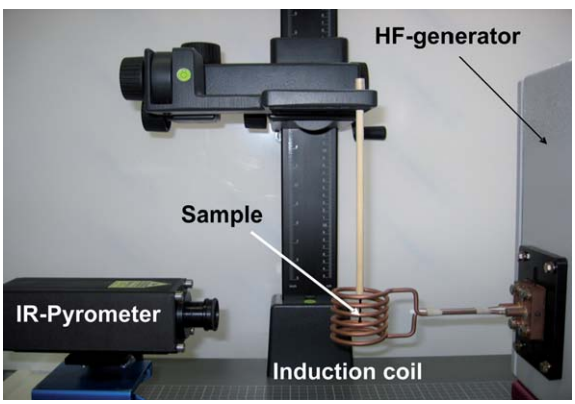

Fig. 1 Experimental setup for inductively triggering SME in an AMF consisting of a high-frequency generator, a water cooled coil with six loops having a diameter of 4 cm, and an IR pyrometer (with kind permission from Springer Science + Business Media: taken from ref. 36).

on the extruder screws are used to achieve homogeneous distribution of nanoparticles into the polymer.[52]

Another way to improve the distribution of MNP in the polymer matrix is the surface coating of MNP with organic or inorganic layers. Surface coating of the MNP prevents agglomeration and enables the stabilization of the individual magnetic cores.[53] In addition, coating of MNP may enhance their biocompatibility. *E.g.* coating of MNP with dextran for hyperthermia to treat oral cancer was reported.[54] Other already approved products for *in vivo* applications based on coated MNP include, *e.g.* treatment of anemia and usage as an MR contrast agent.[55,56] Coating of the MNP with an inorganic layer such as a silica matrix enhanced the compatibility of the MNP with the polymer matrix, reduced the formation of μm-sized agglomerates and supported a homogeneous distribution of MNP within the polymer matrix.[43]

In this manuscript we review memory effects in MNPC. At first, a brief introduction of fundamental power loss mechanisms responsible for magnetic heating of the MNP in an AMF is provided. Magnetically controlled dual- and triple-shape effects of MNPC followed by magnetically adjustable memory effects in dual or triple-shape MNPC are presented. Subsequently, the magnetic-memory effect, which is the capability of the MNPC to remember the magnetic field strength (H), at which it was deformed recently, is described. Finally, a conclusion with potential applications and future directions in the development of MNPC is provided.

2 Heating of magnetic nanoparticles in an AMF

For inductive heating high frequency (typically $f > 10$ MHz) current is used to generate oscillating magnetic fields (H) *via* an induction coil. Three potential heating mechanisms are possible in ferro- or ferrimagnetic nanoparticles: Néel relaxation, Brownian motion relaxation, and hysteresis losses.[57–59] MNP with crystal sizes between 1 and 10 nm allow heating through Brownian or Néel magnetic relaxation and are called superparamagnetic nanoparticles (SPNP). In the Néel relaxation mechanism, the particle's magnetic dipole reorients itself within the particle in response to an externally applied AMF. Heating is caused by the particle's magnetic moment resisting this orientation and is dependent on the particle magnetism.[57] The phenomenon is illustrated in Fig. 2a for polymer nanocomposites containing SPNP. The Néel relaxation time is given by the following equation,

$$\tau_N = \tau_0 e^{\left(\frac{KV}{K_b T}\right)} \quad (3)$$

where τ_0 is a time constant, K_b is the Boltzmann constant, K is an anisotropic constant, V is the volume of the particle core and T is the particle temperature.

A second heating mechanism is Brownian relaxation. Here heating results from the friction between particles which rotate in response to an externally applied AMF and the carrier fluid due to the viscosity effect resisting the particle's rotation. The Brownian relaxation time is given by

$$\tau_B = \frac{3\eta V_H}{K_b T} \quad (4)$$

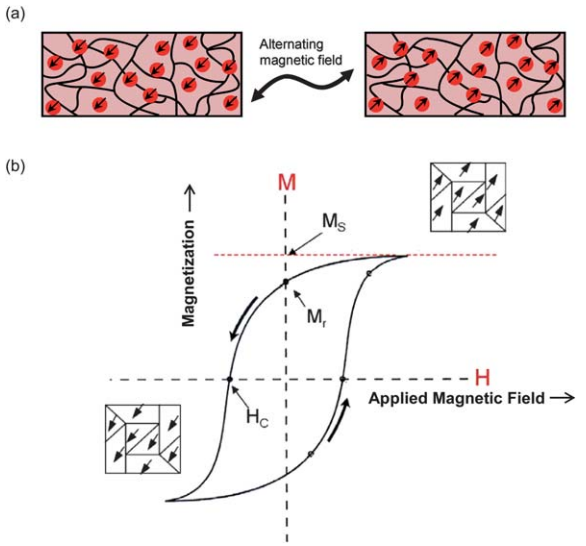

Fig. 2 (a) Néel relaxation process in SPNP incorporated in a polymer matrix. (b) Hysteresis curve for the multidomain magnetic material. M_S is the saturation magnetic limit, M_r is the remnant magnetization at $H = 0$, H_c is the coercivity (adapted with permission from ref. 60, copyright 1996 American Chemical Society).

where η is the viscosity of the carrier fluid and V_H is the hydrodynamic volume of the particle.

The characteristic relaxation times of the particles that ensemble for Néel relaxation or Brownian motion relaxation depend in quite different manners on the mean particle diameter. The power losses due to Néel and Brownian relaxations are approximately given by

$$P = \pi\mu_0\chi_0 H_0^2 f \frac{2\pi f\tau}{1 + (2\pi f\tau)^2} \quad (5)$$

where μ_0 is the permeability of vacuum (1.25×10^{-6} T m A^{-1}), χ_0 is the equilibrium susceptibility, H_0 is the field strength and f is the frequency of the AMF. If the nanoparticle is fixed in a place and unable to rotate, such as when incorporated in a polymer matrix, Brownian motion relaxation will be eliminated and can be neglected for the particle heating.

In addition to relaxational losses, in larger particles with a particle size >20 nm heating can also result from magnetic hysteresis losses, which occur in multi domain ferro- or ferrimagnetic particles exposed to an AMF. Hysteresis is a phenomenon describing the path depending on the magnetic response of magnetic materials to an applied magnetic field. Hysteresis loss can mainly be attributed to the domain wall motion. The generated heat is proportional to the area of the hysteresis loop and the frequency of the AMF. As SPNP have only one magnetic dipole and no domain walls, the hysteresis curve has the shape of a single sigmoidal curve having no area. Therefore, in SPNP no heating by hysteresis will occur. Fig. 2b schematically illustrates a hysteresis loop (applied field *vs.* magnetization).

In principle, the heating power associated with hysteresis losses is higher than that based on Brownian and Néel relaxation. Nevertheless, a high magnetic field, which is beyond the biologically tolerable range, has to be applied. Conversely, these

fields can rarely be used because of physiological and technological restrictions. As no domain wall movements are involved in the case of SPNP, they absorb much more energy at tolerable AC-magnetic fields compared to multidomain particles and are more attractive for *in vivo* applications.[60]

3 Magnetically actuated dual-shape effect

Incorporation of coated MNP into a thermoplastic SMP enabled the magnetically induced dual-shape effect (DSE).[48] The effect was demonstrated for two different thermoplastic materials as the matrix with particle contents up to 40 wt%. The first polymer matrix was an aliphatic polyetherurethane (TFX) from methylene bis(*p*-cyclohexylisocyanate), butanediol, and polytetrahydrofuran while the second was a biodegradable multiblock copolymer (PDC) with poly(*p*-dioxanone) as the hard segment and poly(ε-caprolactone) (PCL) as the switching segment. While PDC contained crystallizable switching segments, TFX provided an amorphous switching phase, which could solidify by vitrification. The chemical structures of TFX and PDC are shown in Fig. 3a and b, respectively.

The magnetic nanoparticles consisted of an iron(III)oxide (Fe_2O_3) core in a silica (SiO_2) matrix (SNP). The mean aggregate size (photon correlation spectroscopy of an aqueous dispersion) was 90 nm, the mean domain size (X-ray diffraction) was 20–26 nm, and the domain content (X-ray fluorescence analysis) was 50–60 wt%.[61]

The SNP were mixed with the SMP matrix at approximately 170 °C resulting in a homogeneous distribution of the SNP in the polymeric matrix as demonstrated by TEM micrographs (Fig. 4). The silica apparently improved the compatibility between the particles and the polymer matrix. The black particles in Fig. 4b are the iron oxide domains embedded into the silica matrix (dark gray wrapping).

Once the magnetic field ($f = 258$ kHz, $H = 30$ kA m^{-1}) was switched on, the temperature of the MNPC increased. Within a few minutes the temperature measured at the sample surface reached a constant level, the maximum achievable temperature T_{max}, as here the sample is in thermal equilibrium with the environment. T_{max} increased strongly with increasing SNP concentration and magnetic field strength. When T_{max} exceeded T_{sw} of the SMP-MNPC, the DSE occurred as illustrated for a TFX based MNPC with 10 wt% SNP (Fig. 5). As the mean

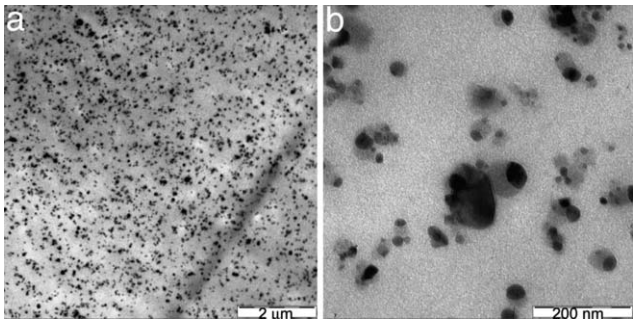

Fig. 4 Transmission electron microscopy images of the nanocomposite from TFX and 10 wt% SNP (taken from ref. 48, copyright 2006 National Academy of Sciences, USA).

domain size of the SNP was slightly higher than 20 nm, hysteresis and/or relaxational losses were assumed to be responsible for heating the nanocomposites under AMF.

It was shown that particle contents between 2.5 and 10 wt% did not influence the thermal properties of the nanocomposites significantly. The effect of MNP on the cyclic, thermomechanical tensile tests of TFX nanocomposites was investigated by comparing TFX and a nanocomposite from TFX and 10 wt% SNP (Fig. 6). In these tests, the samples were elongated at a temperature T_{high}, which was higher than T_{sw} but lower than the thermal transition of the hard segment. Strain was kept constant for a certain time interval to allow relaxation of the strained switching segments. Afterwards the elongated samples were cooled to a temperature T_{low}, which was below T_{sw} to fix the temporary shape. This step was performed under stress control, which resulted in an increase of strain as a consequence of entropy elasticity. Reheating the SMP-MNPC to T_{high} initiated the SME.

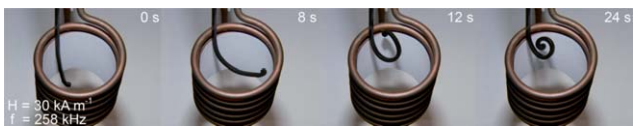

Fig. 5 Magnetically induced SME of a thermoplastic SMP-MNPC from nanoparticles consisting of iron(III)oxide particles in a silica matrix and a polyetherurethane (with kind permission from Springer Science + Business Media: taken from ref. 14).

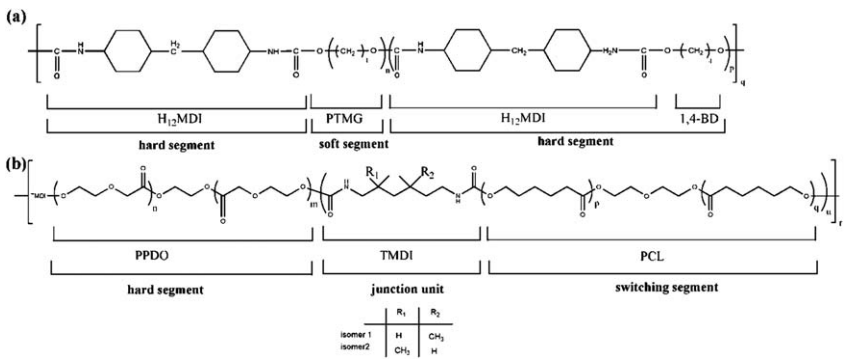

Fig. 3 Chemical structures of thermoplastic SMP. (a) Aliphatic polyetherurethane TFX, which is prepared from methylene bis(*p*-cyclohexylisocyanate) (H12 MDI), 1,4-butanediol (BD), and poly(tetramethylene glycol) (PTMG). (b) Multiblock copolymer PDC consists of PPDO, poly(*p*-dioxanone); TMDI, 2,2(4),4-trimethylhexanediisocyanate; PCL, poly(ε-caprolactone) (taken from ref. 48, copyright 2006 National Academy of Sciences, USA).

The influence of MNP on thermally induced shape-memory properties was quantified by R_f and R_r. For TFX composites R_f values were in the range between 98% and 100% and $R_r \approx 80\%$ was observed regardless of the concentration of the MNP. For PDC samples R_f in the range of 50 and 57% and R_r in the range of 47 and 65% were determined. PDC-based SMP-MNPC differed from the TFX-based samples, as here a deformation at ambient temperature called cold drawing was used to program the samples.

T_{max} of SMP-MNPC was found to be a function of the sample geometry as well as instrumental parameters, *e.g.* amplitude (H) and frequency (f) of the applied AMF. The higher the surface to volume ratio (S/V) of the sample, the lower the T_{max} (Fig. 7a). Another very important factor was the surrounding environment, which influenced the heat loss of the sample and in this way T_{max}. In the majority of cases the SME of the SMP-MNPC was triggered by an AMF in air. As the thermal conductivity of air is relatively low, in this case the amount of heat loss from the sample surface to the environment is negligible. For many potential applications including *in vivo* medical applications, the medium is aqueous in nature having a high thermal conductivity and heat capacity compared to air. Fig. 7b shows the heating curves of a SMP-MNPC from TFX and 18 wt% SNP that was inductively heated in air, in 10 wt% gelatin–water solution, and in distilled water. Apparently only in air the sample temperature exceeded the T_{sw} (74 °C) of the TFX matrix while the increase in temperature in water and gelatin solution was very small.[61]

The frequency and the magnetic field strength required for triggering SME can be reduced by increasing the size of the particles to the micro-size range. Composites from magnetite particles with a diameter of 9 μm and a thermoplastic polyurethane derived from diphenylmethane-4,4′-diidocyanate, adipic acid, ethylene oxide, propylene oxide, 1,4-butanediol and bisphenol A with T_g as T_{trans} were developed by conventional processing methods. The storage modulus increased with the increment of the magnetite volume fraction. Here a low magnetizing frequency of $f = 50$ Hz and a field strength $H = 4.4$ kA m^{-1} were used to actuate the SME owing to the heat generation mechanism involved in microsized magnetite particles. For a sample with 20 vol% particles at a magnetizing frequency of 50 Hz a power loss of $P = 513$ J m^{-3} was calculated. These power losses were converted into heat and a temperature increase of $\Delta T = 6$ K min^{-1} was estimated by heating the sample in a magnetic field at a magnetizing frequency of 50 Hz. However, during magnetic heating at this frequency, the SME occurred much slower, and in a composite sample with 20 vol% particles ($3 \times 3 \times 100$ mm^3) the initiation of recovery was started after 4 min and full recovery at 20 min was observed.[62]

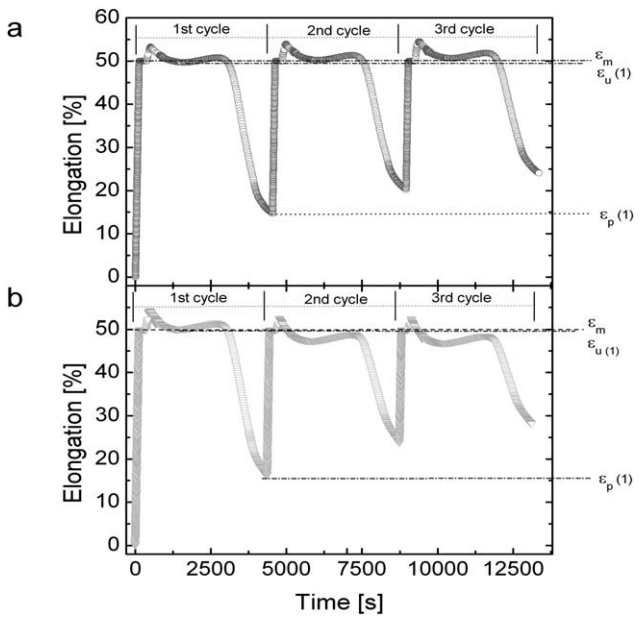

Fig. 6 Results of cyclic thermomechanical tensile tests of TFX materials. $T_{low} = 0$ °C, $T_{high} = 80$ °C, and $\varepsilon_m = 50\%$. (a) TFX; (b) composite from TFX and 7.5 wt% magnetic nanoparticles (taken from ref. 48, copyright 2006 National Academy of Sciences, USA).

An innate thermoregulation of T_{max} was demonstrated in a SMP-MNPC based on shape-memory polyurethane (SMPU, MP5510 from Diaplex Co. Ltd, Tokyo, Japan) and nickel zinc ferrite particles with loading levels of 10 and 20 wt%. If these ferromagnetic particles have an appropriate diameter they generate heat only by the hysteresis loss mechanism, which is limited by the Curie temperature (T_C). Once the material was heated above T_C the ferromagnetic material became paramagnetic and lost its ability to generate heat *via* the hysteresis loss mechanism. Conclusively, the danger of overheating in *in vivo* applications can be eliminated by selecting a ferromagnetic particle material with a T_C within an appropriate temperature interval. However, the temperature achieved during exposure to 10 MHz fields was far below T_C, and a modest temperature rise of 11 °C and 7 °C in 45 s at 20 wt% and 10 wt% particle content, respectively was observed.[47]

Polymerization of reactive monomers or oligomers functionalized with telechelic reactive groups and MNP gives rise to polymer network based composites. An example is the polymerization of poly(ε-caprolactone) diisocyanatoethyldimethacrylate (PCLDIMA) with MNP.[42,63] In these thermosetting composites a fast actuation of the samples was observed, which can be attributed to the polymer network structure of the SMP. However, a challenge is sedimentation of particles during the curing process, which can be circumvented by sufficient viscosity of the precursor mixture.

4 Magnetically controlled triple-shape effect

A magnetically controlled TSE was realized by the incorporation of MNP in TSP. The first example of a multiphase polymer network named as MACL was selected as the matrix material for the magnetically switchable triple-shape composite.[64] MACL composites were composed of PCL and poly(cyclohexylmethacrylate) (PCHMA) segments with SNP as the filler. A series of MACL composites were synthesized by heating and stirring a mixture of precursors, PCLDIMA (30 wt% to 70 wt %), cyclohexylmethacrylate (CHMA) and SNP (0 wt% to 15 wt%) at 75 °C. The thermosets were cured at 80 °C for 24 h using benzyl peroxide (BPO) as the free radical initiator. The nomenclature of the different MACL nanocomposites is provided in Table 1. The high degrees of gel content with values between 96% and 98% indicated that particles did not influence the crosslinking reaction. Microscopic analysis showed a less homogeneous distribution of

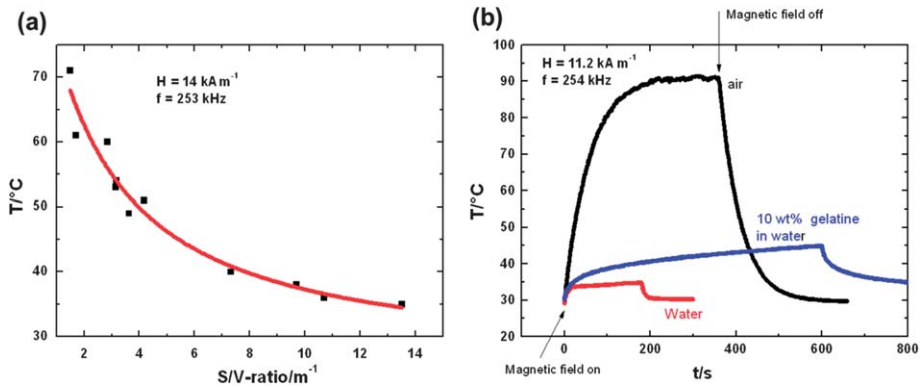

Fig. 7 (a) Surface to volume ratio dependence of the sample's temperature for TFX with 18 wt% magnetic nanoparticles. The temperature was determined as the bulk temperature utilizing a thermocouple. (b) Inductively heating curves for TFX with 18 wt% MNP in different mediums ($f = 254$ kHz and $H = 11.2$ kA m^{-1}) (taken from ref. 61 with kind permission, copyright 2009 IOP Publishing Ltd).

the nanoparticles and few micro-sized agglomerates were observed. The existence of segregated phases as required for the triple-shape effect was confirmed by dynamic mechanical thermal analysis (DMTA) at varied temperatures. The different thermal transitions were associated with amorphous PCL, crystalline PCL and amorphous PCHMA phases. The network composites exhibited two distinct, well separated thermal transitions, a melting transition assigned to the crystalline PCL domains in the range of 41 °C to 48 °C and a glass transition associated with the amorphous PCHMA domains in the range of 131 °C to 156 °C. Furthermore, a T_g of the amorphous PCL phase $T_{g,PCL}$ was determined in the range of −69 °C to −55 °C. These thermal transition temperatures did not vary with the composition (PCL to PCHMA weight ratio) so that TSE could be triggered at the same magnetic field strength H.[64]

MNPC samples with SNP concentrations in the range from 10 wt% to 15 wt% were selected to achieve temperatures up to 150 °C in the magnetic field. As described in the third section, the magnetic field strength required to reach T_{max} will change, if the surface area to volume (S/V) ratio of the sample is changed. Therefore bending experiments were performed to ensure precise control of the desired temperatures for the test specimen during TSE initiation in the magnetic field. During bending, the S/V ratio remains almost constant and additional heating effects caused by changes in the S/V ratio for elongated samples should be minimized.

To find out T_{max} of the non-deformed MACL composites, the samples were exposed to AMF by increasing H stepwise. Only samples containing 12.5 wt% and 15 wt% nanoparticles were able to reach the $T_{max} = T_{high} = 150$ °C, which was necessary to achieve the recovery of the original shape of the MACL polymer network. In addition the magnetic field strengths of $H_B = 14.6$ kA m^{-1} to reach the $T_{mid} = 70$ °C and $H_C = 29.4$ kA m^{-1} for complete recovery of shape C at $T_{high} = 150$ °C were determined.

Three different types of triple-shape experiments were designed, in which the applied deformation during TCP was bending for the examination of triple-shape properties in the magnetic field.

Two different thermomechanical procedures, a two-step TCP (TCP-2s) and a single step TCP (TCP-1s), were used for creating shapes B and A, respectively, followed by sequential recovery in the magnetic fields at $H_B = 14.6$ kA m^{-1} and $H_C = 29.4$ kA m^{-1}. A schematic representation of the different TCPs is shown in Fig. 8.

Table 1 Triple-shape properties of MACL based polymer network composites determined by applying different TCPs and recovery in the AMF with $f = 258$ kHz and at $H = 14.6$ kA m^{-1} and $H = 29.4$ kA m^{-1} to shape C (reproduced from ref. 64 with permission from The Royal Society of Chemistry)

	Shape fixity ratios			Shape recovery ratios	
Sample ID[a]	R_f(C → B) [%]	R_f(B → A) [%]	R_f(C → A) [%]	R_r(A → B) [%]	R_r(A → C) [%]
MACL(30)C125[c]	100	77	77	74	93
MACL(40)C125[c]	91	89	89	97	95
MACL(50)C125[c]	61	100	100	100	97
MACL(60)C125[c]	42	100	100	100	98
MACL(70)C125[c]	14	100	100	100	100
MACL(30)C125[d]	91	87	87	46	100
MACL(40)C125[d]	67	94	94	67	100
MACL(50)C125[d]	34	94	94	82	100
MACL(60)C125[d]	23	99	99	88	100
MACL(70)C125[d]	6	100	100	94	100
MACL(40)C125[e]	n.d.[b]	n.d.[b]	100	55	100

[a] The two-digit numbers in parentheses given for the sample IDs are the contents of PCLDIMA in the starting material mixture of the organic compounds in wt% and the last three digits represent the 12.5 wt% of added nanoparticles. [b] n.d. = not determined during single step TCP R_f(C → B) and R_f(B → A). [c] Results obtained for the programming method TCP-2s-I. [d] TCP-2s-II. [e] Results from TCP-1s.

During TCP-2s-I the original straight sample (shape C; θ_C) was deformed at T_{high} = 150 °C, where the polymer matrix is completely amorphous, by bending to an angle of $\theta_B^\circ = 90^\circ$. When cooled to T_{mid} = 70 °C, while keeping the external strain constant, the first temporary shape B (θ_B) was fixed by vitrification of the PCHMA domains. In the next step the sample was subsequently bent to $\theta_A^\circ = 180^\circ$. Cooling to $T_{low} = -10$ °C under load fixed shape A (θ_A), which was obtained after releasing the stress, by crystallization of the PCL domains. For magnetic field recovery experiments the programmed sample (shape A) was exposed to H_B = 14.6 kA m^{-1} representing T_{mid} = 70 °C and afterwards to H_C = 29.4 kA m^{-1} corresponding to T_{high} = 150 °C. In this test the recovery of shape B was characterized by the bending angle achieved at T_{mid}(θ_B^{rec}) while shape C was related to θ_C^{rec} observed at T_{high}.

In TCP-2s-II shape B was achieved by cooling from T_{high} = 150 °C to $T_{low} = -10$ °C. Here θ_B° was fixed by two processes: vitrification of the PCHMA domains and crystallization of PCL domains. After heating to T_{mid} = 70 °C θ_A was created as described in TCP-2s-I.

The TSE of all samples was quantified by determining the strain fixity ratios R_f(C → B), R_f(B → A), and R_f(C → A) and the shape recovery ratios R_r(A → B) and R_r(A → C). All MACL composites exhibited pronounced triple-shape properties when activated in the AMF as shown in Table 1.

The triple-shape properties of MACL(040)C12 were investigated by a single-step process TCP-1s in addition to the two-step processes TCP-2s-I and TCP-2s-II. In this process shape A (θ_A) was realized by deformation to $\theta_A^\circ = 180^\circ$ at T_{high} = 150 °C and subsequent cooling to $T_{low} = -10$ °C.

All TCPs resulted in complete fixation of shape A independent of the composition, while fixation of shape B was found to decrease significantly with rising PCLDIMA content.

A pronounced TSE was observed for nanocomposites with PCLDIMA weight fractions between 30 wt% and 50 wt%, when module 1 was applied. An almost complete recovery of shape C was achieved at H_C = 29.4 kA m^{-1} with $T_{max} \approx 150$ °C for all materials, while at H_B = 14.6 kA m^{-1} with $T_{max} \approx 70$ °C, the values for R_r(A → B) increased with increasing PCDIMA content. Fig. 9 shows the images taken at H = 0 kA m^{-1}, H_B = 14.6 kA m^{-1}, and H_C = 29 kA m^{-1} obtained during the recovery of MACL(40)C125 after applying the different TCP modules.

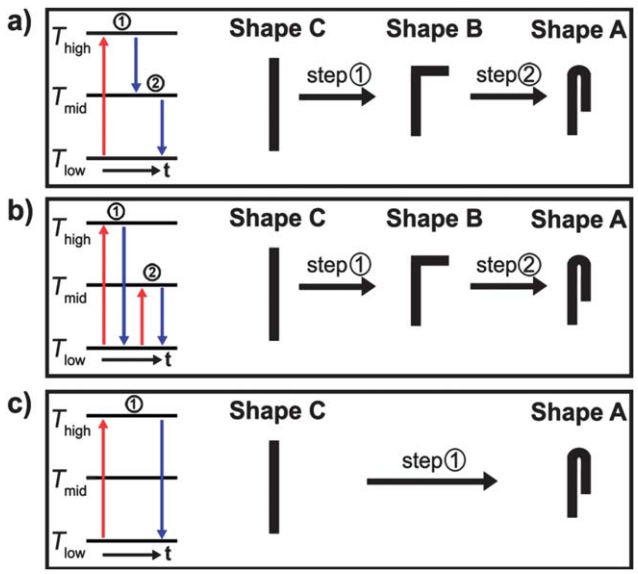

Fig. 8 Schematic representation of the different triple shape creation procedures applied, (a) TCP-2s-I, (b) TCP-2s-II, (c) TCP-1s (reproduced from ref. 64 with permission from The Royal Society of Chemistry).

The triple-shape capability of the MACL nanocomposites programmed by TCP-2s-1 was also monitored by increasing the magnetic field strength stepwise (ΔH = 1 kA m^{-1}) from H = 0 kA m^{-1} to H = 29.4 kA m^{-1}, which resulted in the surface temperature increase around 3 to 4 K for each step. The recovery behavior of the nanocomposites depended strongly on the composition of the polymer matrix. A pronounced TSE characterized by a clearly separated two-step change in shape with increasing H was observed only for MACL(40)C125. Here, two separate switching field strengths for recovery of shapes B and C were determined at $H_{sw,1}$(A → B) = 10.4 kA m^{-1} and $H_{sw,2}$(B → C) = 20.0 kA m^{-1}, respectively. Samples with higher PCLDIMA content (*e.g.* MACL(70)C125) displayed only dual-shape capability. It was concluded that the composition of the polymer matrix is an essential parameter for realization of triple-shape capability. These observations clearly demonstrated the sensible balance between the crystalline PCL domains responsible for fixation of shape A and the glassy PCHMA domains fixing shape B.

In addition to MACL composites, the magnetically controlled triple shape-capability of multiphase polymer networks named CLEG with two crystallizable switching segments based on poly(ethylene glycol) (PEG) side chains and PCL crosslinks was demonstrated.[65] Here, $T_{trans,A}$ and $T_{trans,B}$ are melting temperatures. A series of MNPC were prepared by reacting various ratios of poly(ethylene glycol)monomethyl ether monomethacrylate (PEGMA) and PCLDIMA crosslinker in the presence of 2.5 to 10 wt% of SNP. All CLEG based MNPC exhibited two well separated thermal transitions, $T_{m,PCL}$ = 51 °C attributed to PCL domains and $T_{m,PEG}$ ranging from 38 to 20 °C related to the crystalline PEG domains, which decreased with increasing PCL content. Application of two-step programming procedures resulted in excellent triple-shape properties in samples containing 30 and 40 wt% of PCLDIMA in the starting reaction mixture. When a TCP-1s was applied for programming, all samples independent of the composition displayed only a dual-shape behavior. This behavior can be explained with the polymer network structure, in which only the PCL-segments contribute to the polymer network and in this way determine the elasticity.

5 Adjusting the apparent switching temperature ($T_{sw,app}$) of the nanocomposites by a magnetic field

A particular challenge in the context of the numerous biomedical applications for SMP, *e.g.* as potential implant materials for minimally invasive surgery or drug release systems, is the precise control of the material's function, for example, the switching bulk temperature $T_{sw,bulk}$. Depending on the various application scenarios $T_{sw,bulk}$, which is associated with T_{trans} (T_m or T_g) of the switching domains, needs to be adjusted to the application relevant temperature. One strategy is the variation of T_{trans} by adjusting the molecular architecture, *e.g.* variation of comonomer ratios in AB polymer networks, molecular weight of the

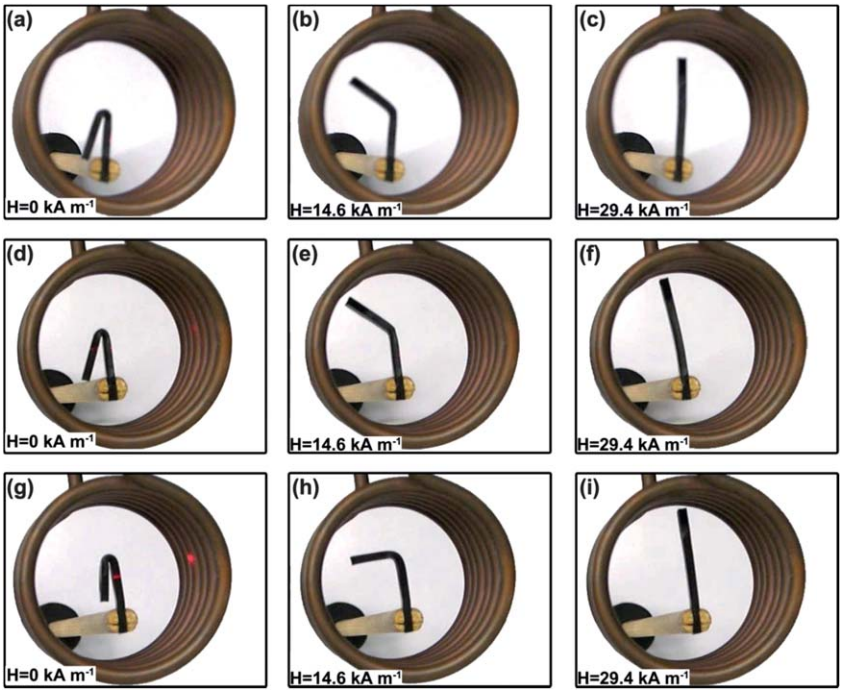

Fig. 9 Images obtained for MACL(40)C125 during recovery at magnetic field strength H of 0 kA m^{-1}, 14.6 kA m^{-1} and 29.4 kA m^{-1}. (a)–(c): TCP-2s-I; (a) shape A at 0 kA m^{-1}; (b) shape B at 14.6 kA m^{-1} and (c) shape C at 29.4 kA m^{-1}. (d)–(f): TCP-2s-II; (d) shape A at 0 kA m^{-1}; (e) shape B at 14.6 kA m^{-1} and (f) shape C at 29.4 kA m^{-1}. (g)–(i): TCP-1s; (g) shape A at 0 kA m^{-1}; (h) shape B at 14.6 kA m^{-1} and (i) shape C at 29.4 kA m^{-1} (reproduced from ref. 64 with permission from The Royal Society of Chemistry).

precursors used as starting materials, crosslinking density *etc.*[66,67] A $T_{sw,bulk}$ slightly above the body temperature enabled on demand the control of the shape change by short time application of heat either indirectly through IR-irradiation or directly by using an external heating medium, for example through a catheter.[1,66] Instead of varying $T_{sw,bulk}$, another strategy is the adjustment of the $T_{sw,app}$ determined as the environmental temperature (T_{env}) as demonstrated for MNPC with dual- or triple-shape capabilities recently. Here, a combination of environmental heating (T_{env}) and magnetic heating was used to reversibly tailor the $T_{sw,app}$.[68] This method could help to avoid the laborious synthesis of SMP with different T_{sw} tailored for specific applications.

The influence of combined (environmental and magnetic) heating was explored for three different MNPC, based on a dual-shape or a triple-shape polymer as the matrix. The sample with the dual-shape matrix polymer named CLC05 was prepared by crosslinking crystallizable PCLDIMA in the presence of 5 wt% SNP. The MNPC named as CLEGC05 and CLEGC10 having a triple-shape polymer as the matrix were obtained by copolymerization of PEGMA (60 wt%) with PCLDIMA in the presence of 5 wt% and 10 wt% SNP. CLC05 showed an H_{sw} at 26.6 kA m^{-1}, while for triple-shape nanocomposites two H_{sw} were obtained at $H_{sw}(A \rightarrow B) = 20.2$ kA m^{-1} and $H_{sw}(B \rightarrow C) = 24.8$ kA m^{-1} for CLEGC05, whereas CLEGC10 exhibited significantly lower values of $H_{sw}(A \rightarrow B) = 16.1$ kA m^{-1} and $H_{sw}(B \rightarrow C) = 20.2$ kA m^{-1}, because of the higher SNP weight content.

The influence of the environment combined with inductive heating on T_{bulk} was explored in magnetic and environmental heating experiments. In magnetic heating experiments H was varied in a stepwise increase from $H_0 = 0$ kA m^{-1} to $H_{max} = 29.4$ kA m^{-1} at a constant frequency of $f = 258$ kHz and constant T_{env}.

In environmental heating experiments T_{env} was varied from ambient temperature to 57 ± 2 °C, while H and f were kept constant. Here, the selected values of applied H were less than H_{sw} for both dual and triple-shape MNPC. For CLEGC10, $H_1 = 13.2$ kA m^{-1}, $H_2 = 15.1$ kA m^{-1} and $H_3 = 18.2$ kA m^{-1} were applied, which were below $H_{sw}(B \rightarrow C) = 20.2$ kA m^{-1}, while for MNPC with 5 wt% nanoparticle content (CLC05, CLEGC05) $H_3 = 18.2$ kA m^{-1}, $H_4 = 20.2$ kA m^{-1}, and $H_5 = 24.0$ kA m^{-1} < $H_{sw}(B \rightarrow C) = 24.8$ kA m^{-1} were used. A simple model was proposed to explain the T_{bulk} achieved by combined environmental and magnetic heating as $T_{bulk} = T_{env} + \Delta T_{mag}$ with $\Delta T_{mag} = kH^2$, where k is a material related constant, which depends on several factors (*e.g.*, heat conductivity of the polymer matrix, magnetic properties of the particle, their weight content, and aspect ratio). A correlation of T_{bulk} to H by the power of two was observed during magnetic heating experiments carried out at different constant T_{env} (Fig. 10a–c). In addition, a similar k value could be determined for different MNPC (CLC05, CLEGC05) with the same MNP content, while for CLEGC10 higher values of k were obtained indicating that T_{bulk} increased with increasing MNP weight content. In contrast, during the environmental heating experiment a linear correlation between T_{bulk} and T_{env} was observed for all investigated MNPC (Fig. 10d–f). T_{bulk} was systematically increased by increasing the value of constant H by the inductive heating contribution ΔT_{mag}. However, it was observed that ΔT_{mag} decreased with increasing T_{env}. This decrease in ΔT_{mag} was attributed to the temperature-dependent relaxation process related to the hysteresis loss, which are

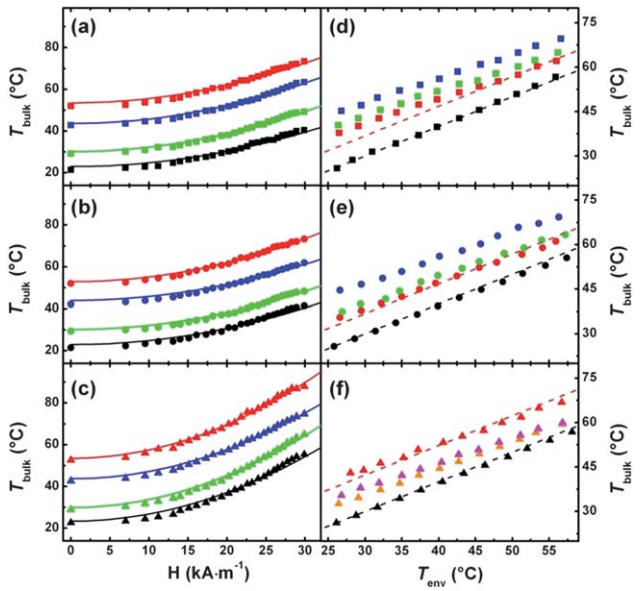

Fig. 10 Bulk temperatures (T_{bulk}) obtained for dual- and triple-shape nanocomposites (CLC05: square symbols, CLEGC05: circle symbols and CLEGC10: triangle symbols) during: (a–c) magnetic heating at different constant T_{env} (22 °C: black; 30 °C: green; 43 °C: blue; and 56 °C: red). Curves are fitted according to the model $T_{bulk} = kH^2 + T_{env}$ with k as the fit variable (solid lines); (d–f) environmental heating at different H (H_0 = 0 kA m^{-1}: black symbols; H_1 = 13.2 kA m^{-1}: orange symbols; H_2 = 15.1 kA m^{-1}: magenta symbols; H_3 = 18.2 kA m^{-1}: red symbols; H_4 = 20.2 kA m^{-1}: green symbols; and H_5 = 24.0 kA m^{-1}: blue symbols). The dashed black lines represent $T_{env} = T_{bulk}$ at H_0, while the dashed red lines are model calculations for H_3 according to the above mentioned model using averaged k-values determined in magnetic heating experiments (taken from ref. 68, copyright 2011 Wiley-VCH Verlag GmbH & Co. KGaA, Weinheim).

responsible for the inductive heating of the MNP, or to the structural changes in the polymer matrix such as melting of crystalline domains.

The thermally induced SME supported by a weak magnetic field was investigated in bending experiments to minimize changes in the S/V ratio during shape-recovery. For dual shape MNPC CLC05, a single step DSCP was applied, while for triple-shape materials CLEGC05 and CLEGC10, a two step TCP was applied. Shape recovery experiments were conducted with programmed samples by increasing T_{env} stepwise from ambient temperature to 57 °C at constant $H < H_{sw}$. Shape-memory properties were quantified by determining the change in the deformation angle during programming and recovery.[65] Here, the change in the bending angle ($\Delta\theta_{rec}$) during recovery depending on T_{env} and T_{bulk} was analyzed for the determination of $T_{sw,app}$ and $T_{sw,bulk}$ (Fig. 11).

A systematic decrease in $T_{sw,app}(A \rightarrow C) = 54 \pm 2$ °C without the magnetic field to $T_{sw,app}(A \rightarrow C) = 41 \pm 2$ °C at H_5 (Fig. 10a) was observed for dual-shape MNPC CLC05. In contrast, $T_{sw,bulk}(A \rightarrow C)$ remained almost unchanged at $T_{sw,bulk}(A \rightarrow C) = 55 \pm 2$ °C. In the case of triple-shape MNPC CLEGC05 and CLEGC10, both $T_{sw,app}(A \rightarrow B)$ and $T_{sw,app}(B \rightarrow C)$ were systematically lowered by applying the magnetic field H_1 to H_5 (Fig. 11b and c), while $T_{sw,bulk}(A \rightarrow B) = 45 \pm 3$ °C and $T_{sw,bulk}(B \rightarrow C) = 56 \pm 3$ °C (Fig. 11e and f) were constant.

The applicability of the concept of magnetically adjustable $T_{sw,app}$ was demonstrated by a fixation device with a triple-shape CLEGC05 hook as a magnetosensitive active component and a solely thermosensitive fixation counterpart fabricated from a PCLDIMA based dual-shape polymer network (CL) with $T_{sw,CL} = 47 \pm 2$ °C. A schematic representation of the DSCP for CL and TCP for CLEGC05 and the working principle of the fixation device are shown in Fig. 12a and b. The magnetosensitive hook had to enter the hole of the fixation counterpart by changing the shape (A → B) and being locked in shape (B → C) before T_{sw} of the thermosensitive counterpart was reached by increasing the environmental temperature (T_{env}), which causes the fixation counterpart to be lifted upwards to achieve the permanent shape. Here, the challenge was to decrease the $T_{sw,app}(A \rightarrow B)$ and $T_{sw,app}(B \rightarrow C)$ for the triple-shape MNPC below the T_{sw} of the thermosensitive counterpart. This adjustment could be reached by application of an AMF during the environmental heating procedure. Different recovery protocols were performed, which included (1) environmental heating at H_4 = 20.2 kA m^{-1}, (2) environmental heating without the magnetic field, (3) magnetic heating at H_{max} = 29.4 kA m^{-1}, (4) magnetic heating at H_4 and ambient temperature to recover shape B, followed by environmental heating at H = 0 kA m^{-1} to recover shape C. Among the four recovery protocols, only in recovery experiment (1) the CLEGC05 was placed and fixed successfully inside the fixation counterpart before it moved upwards, when T_{env} exceeded $T_{sw,CL}$. Application of H_4 lowered both $T_{sw,app}(A \rightarrow B)$ and $T_{sw,app}(B \rightarrow C)$ below $T_{sw,CL}$. In contrast, all other recovery

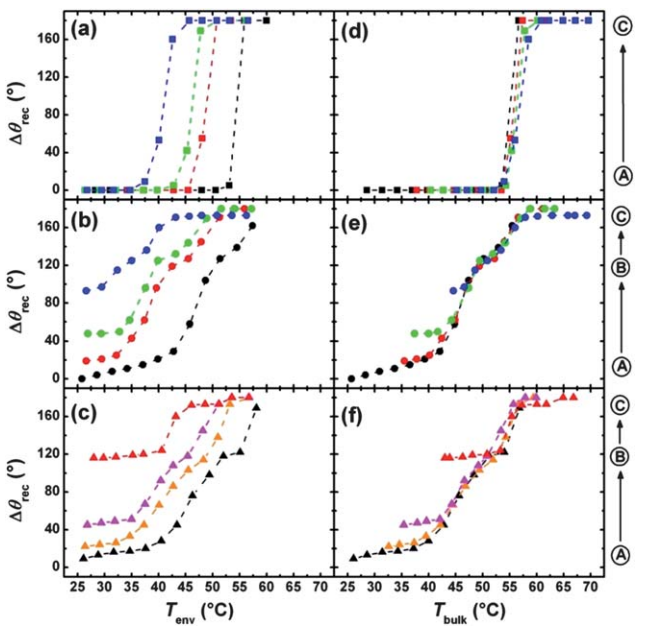

Fig. 11 Change in the bending angle during recovery $\Delta\theta_{rec}$ *versus* T_{env} (a–c) or T_{bulk} (d–f) obtained for dual- and triple-shape nanocomposites (CLC05: square symbols, CLEGC05: circle symbols, and CLEGC10: triangle symbols) during environmental heating at different magnetic field strengths (H_0 = 0 kA m^{-1}: black symbols; H_1 = 13.2 kA m^{-1}: orange symbols; H_2 = 15.1 kA m^{-1}: magenta symbols; H_3 = 18.2 kA m^{-1}: red symbols; H_4 = 20.2 kA m^{-1}: green symbols; and H_5 = 24.0 kA m^{-1}: blue symbols) (taken from ref. 68, copyright 2011 Wiley-VCH Verlag GmbH & Co. KGaA, Weinheim).

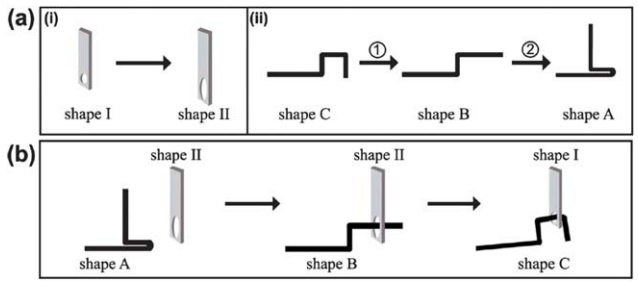

Fig. 12 Fixation device demonstrator consisting of a triple-shape nanocomposite with adjustable $T_{sw,app}$ as the active component. (a) Schematic representation of one step DSCP applied for CL05 (i) and a two-step TCP for CLEGC05 (ii). (b) Working principle of the fixation device (taken from ref. 68, copyright 2011 Wiley-VCH Verlag GmbH & Co. KGaA, Weinheim).

approaches failed. Based on these findings it was speculated that combining two different heating sources for the adjustment of T_{bulk} in the thermosensitive polymers and composites thereof could be extended to other combinations of MNPC, for example, infrared light and T_{env} or microwaves and T_{env}.[68]

6 Nanocomposites with magnetic-memory capability

Incorporation of MNP in temperature-memory polymer matrices extended the concept of a temperature-memory effect (TME), which relies on tailoring the T_{sw} by using broad thermal transitions (ΔT_g or ΔT_m) to a magnetic-memory effect (MME). The MME is defined as the ability of magneto-sensitive materials to remember the magnetic field strength (H_{def}) at which they were deformed recently.[69] The MME requires programming (and recovery) of the MNPC during application of an AMF. The MME was explored in cyclic, magneto-mechanical experiments (CMME), in which MNPC samples were elongated to ε_m while being exposed to H_{def}. The recovery of the MNPC was carried out under stress-free or strain-controlled conditions by increasing the applied H stepwise. Under stress-free conditions MNPC recover their initial shape at a switching magnetic field strength H_{sw} close to H_{def} while under constant strain conditions they respond by building up stress with a peak maximum at $H_{\sigma,max}$.

The MME was investigated in two temperature-memory MNPC (TM-MNPC) with crystallizable or amorphous controlling units. The crystallizable TM-MNPC was based on a binary mixture of two different poly[ethylene-*ran*-(vinyl acetate)] s (PEVA) differing in their comonomer ratio and SNP. The PEVA based MNPC (cPEVA) exhibited a broad T_m ($\Delta T_m = 100$ °C) with a maximum in the range between 92 °C and 96 °C. The amorphous system was a temperature-memory polyurethane (TMPU), in which SNP were dispersed. The TMPU based nanocomposites provided vitrifiable switching domains and exhibited a broad T_g (in the range from 20 to 90 °C) with a maximum at around 74 °C. Incorporation of the SNP did not significantly affect the thermal and mechanical properties of both MNPC.

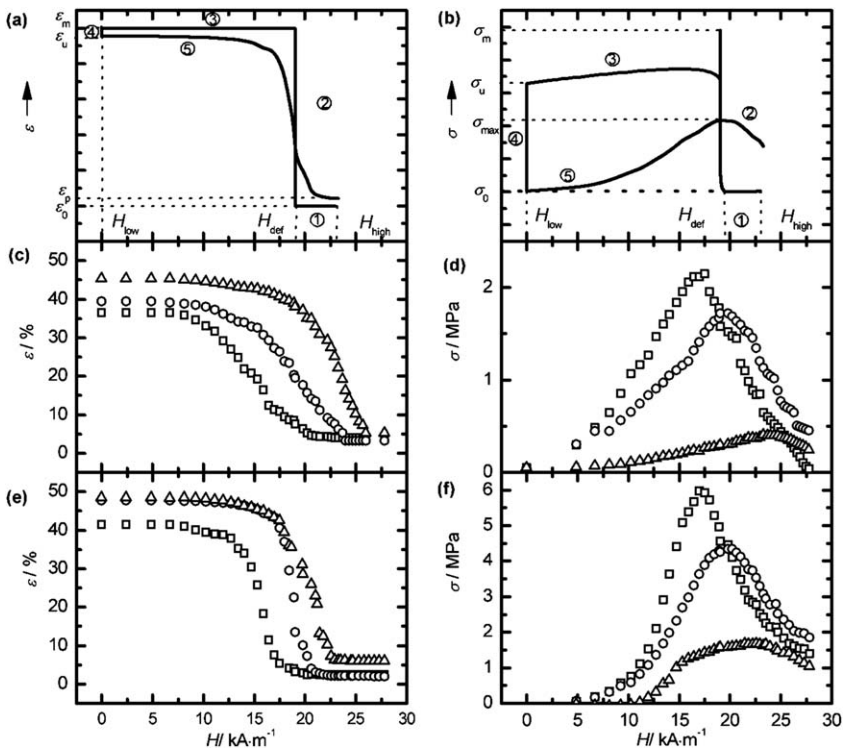

Fig. 13 (a) Strain–magnetic field plot for TMPU(15.1) during the stress-free recovery. (b) Stress–magnetic field plot for TMPU(15.1) during the strain-controlled recovery. (c) Strain recovery curves for cPEVA(13.6) under stress-free recovery conditions. □ for $H_{def} = 15$ kA m^{-1}, ○ for $H_{def} = 19$ kA m^{-1}, and Δ for $H_{def} = 23$ kA m^{-1}. (d) Stress generated for cPEVA(13.6) programmed at three different H_{def} under strain-controlled recovery. (e) Strain recovery curves for TMPU(15.1) under stress-free recovery conditions. (f) Stress generated for TMPU(15.1) programmed at three different H_{def} under strain-controlled recovery conditions (taken from ref. 69, copyright 2012 Wiley-VCH Verlag GmbH & Co. KGaA, Weinheim).

Table 2 Magnetic-memory properties of the nanocomposites (taken from ref. 69, copyright 2012 Wiley-VCH Verlag GmbH & Co. KGaA, Weinheim)

Sample ID	H_{def}[a] [kA m^{-1}]	R_f[b] [%]	R_r[c] [%]	$E_{H(prog)}$[d] [MPa]	$H_{\sigma,max}$[e] [kA m^{-1}]	σ_{max}[f] [MPa]	H_{sw}[g] [kA m^{-1}]
cPEVA(13.6)	15	72 ± 2	89 ± 8	3.9 ± 2	17.0 ± 0.4	2.2 ± 0.3	14.7 ± 0.5
	17	76 ± 1	88 ± 2	2.8 ± 2	18.4 ± 0.3	2.0 ± 0.1	15.3 ± 0.4
	19	79 ± 3	90 ± 7	1.7 ± 1	19.4 ± 0.1	1.7 ± 0.1	18.8 ± 0.5
	21	83 ± 1	92 ± 3	1.0 ± 1	20.6 ± 0.2	0.9 ± 0.2	21.0 ± 0.3
	23	90 ± 1	86 ± 3	0.8 ± 2	23.0 ± 0.6	0.4 ± 0.1	22.6 ± 0.6
TMPU(15.1)	15	83 ± 4	95 ± 6	61.7 ± 5	17.0 ± 0.6	6.0 ± 0.5	16.0 ± 0.4
	17	90 ± 2	90 ± 2	33.0 ± 5	18.4 ± 0.3	5.3 ± 0.3	17.5 ± 0.3
	19	95 ± 1	96 ± 5	16.0 ± 2	19.0 ± 0.5	4.4 ± 0.2	19.0 ± 0.2
	21	94 ± 2	92 ± 2	8.0 ± 3	21.4 ± 0.2	3.9 ± 0.2	19.3 ± 0.1
	23	97 ± 1	87 ± 5	4.6 ± 2	22.5 ± 0.6	1.7 ± 0.2	19.5 ± 0.3

[a] Values of H used for programming the nanocomposites. [b] Shape fixity rate. [c] Shape recovery rate. [d] Young's modulus at H_{def} determined during the tensile tests. [e] Magnetic field strength at stress maximum during strain control recovery. [f] Maximum stress at the corresponding $H_{\sigma,max}$. [g] Switching magnetic field strength during stress-free recovery.

The inductive heating of the nanocomposites was accomplished by positioning the samples in an AMF at a $f = 258$ kHz, while the programmed stretching and recovery under the effect of the magnetic field was controlled by a tensile tester. In contrast to bending experiments (see above) the extent of deformation to ε_m by stretching was geometrically limited by the height of the induction coil. From the magnetic heating of the non-deformed samples, H in a range of 15 to 23 kA m^{-1} was applied and T_{max} was recorded. However, during stretching T_{max} of the sample decreased as it depends on the S/V ratio of the MNPC. In order to minimize the decrease in T_{max} a low value of $\varepsilon_m = 50\%$ was applied, at which the decrease in T_{max} was negligible.

The selection of suitable MNPC for the exploration of the MME was based on the thermal and magnetic properties of the MNPC as the temperature increase from ambient temperature to T_{max} depends on the square of H. Samples cPEVA(13.6) and TMPU(15.1) containing 13.6 wt% and 15.1 wt% SNP were selected as suitable composite materials to explore MME, as they show a maximum ΔT_{trans} (ΔT_g or ΔT_m) and the best fit of the experimentally adjustable range of H between 15 kA m^{-1} and 23 kA m^{-1}. The MME was characterized in the stress-free recovery experiment by switching the field strength H_{sw}, which was determined as the inflection point in the recovery curve. In contrast, in the strain-controlled experiment $H_{\sigma,max}$ was determined as H at the peak maximum stress σ_{max} during recovery.

Fig. 13a illustrates schematically a strain–magnetic field strength plot of TMPU(15.1) deformed at $H_{def} = 19$ kA m^{-1} under stress-free recovery, from which the correlation of the inflection point of the recovery curve H_{sw} with H_{def} can be seen. The stress–magnetic field strength plot of TMPU(15.1) deformed at $H_{def} = 19$ kA m^{-1} under strain-controlled recovery conditions is displayed in Fig. 13b. In cPEVA based MNPC the fraction of crystalline domains with $T_m < T_{max}$ at H_{def} fixed the mechanical deformation to ε_m. In addition, the fixation of the deformation of the cPEVA based MNPC might be enhanced by strain-induced crystallization. However, in the case of TMPU composites the fraction of the amorphous domains associated with the $T_{g,mix}$, which were in the viscoelastic state at H_{def} fixed the mechanical deformation predominantly. On the other hand the amorphous domains of the mixed phase remaining in the vitrified state at

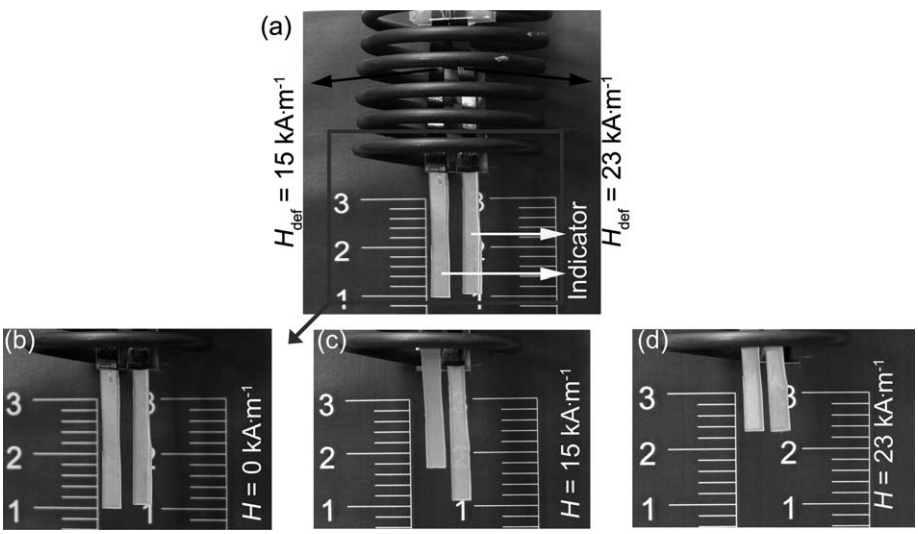

Fig. 14 Macroscopic demonstration of MME in TMPU(15.1). (a) Samples after deformation at $H_{def} = 15$ kA m^{-1} (left) and $H_{def} = 23$ kA m^{-1} (right) with a pure TMPU strip acting as an indicator. (b) Closer view of the indicator. (c) Shape change of the left sample at $H_{def} = 15$ kA m^{-1}. (d) Both samples recovered at $H_{def} = 23$ kA m^{-1} (taken from ref. 69, copyright 2012 Wiley-VCH Verlag GmbH & Co. KGaA, Weinheim).

H_{def} backed the permanent shape and therefore added to an almost complete recovery. The recovery curves of the MNPC under strain-controlled and stress-free recovery conditions are provided in Fig. 13c–f while the magnetic-memory properties are provided in Table 2. A MME with an almost linear correlation between H_{def} and H_{sw} or $H_{\sigma,max}$ could be observed in both MNPC. For the amorphous thermoplastic system a small deviation from the linear relationship was noted under stress-free recovery conditions at high H_{def}.

Finally, a MME for a magneto-sensitive, programmable double switch was demonstrated. Here two TMPU(15.1) samples were deformed to $\varepsilon_m = 50\%$, the first at $H_{def} = 15$ kA m^{-1} and the second at $H_{def} = 23$ kA m^{-1}. The deformations were fixed by reducing H_{def} to 0 kA m^{-1}. When the magnetic field of $H = 15$ kA m^{-1} was applied, the sample programmed at 15 kA m^{-1} was recovered. When H was subsequently increased to $H = 23$ kA m^{-1}, both samples were completely recovered (Fig. 14).[69]

While on one hand the MME requires conditions, such as sample dimension or environmental temperature, which are more defined as compared to the TME, on the other hand the MME enables a remote actuation and an actuation interval, which can be significantly shorter.

7 Conclusion and outlook

Actuation of SMP by AMF was shown to be an interesting technology for remote actuation of the SME, particularly when a direct thermal actuation is not possible. The obtained shape recovery rates of SMP-MNPC by magnetically induced actuation were comparable with those achieved by environmental heating. When SNP were used as fillers high degrees of compatibility and dispersibility of the MNP in the polymer matrices could be achieved. T_{max} of SMP-MNPC was found to be a function of the sample geometry as well as experimental parameters, *e.g.* amplitude (H) and frequency (f) of the applied AMF. A fast actuation was observed in thermosetting nanocomposites, which was attributed to the polymer network structure and the narrow transition temperature. An innate thermoregulation of T_{max} of the SMP-MNPC could be obtained when particles with adjustable T_C are used. The incorporation of SNP in a multiphase polymer network enabled nanocomposites with triple-shape capability. Well separated thermal transitions and suitable thermomechanical programming of the nanocomposites were necessary to observe a pronounced TSE controlled by a magnetic field as discussed for the difference between elongation and bending experiments. A reversible tailoring of the $T_{sw,app}$ in MNPC with dual and triple-shape capabilities was achieved by combining the environmental and magnetic heating as demonstrated by a fixation device with a triple-shape hook as the magnetosensitive active component. This method of reversible tuning of T_{sw} could help to avoid additional synthesis of different SMP-MNPC with T_{sw} tailored to the demands of specific applications. Finally, the MME, which is the capability of the MNPC to remember the magnetic field strengths, which was initially applied for deforming the MNPC, was discussed. The MME required programming (and recovery) of the MNPC by magnetic heating in contrast to the magnetically induced dual and triple-shape effects in which samples are typically programmed by increasing T_{env}. The TMP based MNPC exhibited excellent magnetic-memory properties in the range of H_{def} from 15 kA m^{-1} to 23 kA m^{-1}.

MNPC are examples of functional nanostructured materials with an application potential ranging from electromagnetic interference shielding, magneto-optical storage, biomedical sensing, to flexible electronics.[70,71] The shape-memory functionality in SMP-MNPC increased the versatility of their technical potential. According to the actual demand SMP-MNPC could be properly designed, fabricated, and tailored to meet various applications in many fields such as biomedical devices, drug delivery, biomimetic, robots, switches, or sensors.[5,48] Along with inductive heating capability, MNP as the filler improved the mechanical properties of the MNPC. However, a control over the dispersion of the MNP and their attractive interfacial interactions with the SMP matrix is critical and challenging. To achieve excellent dispersion, the competition between polymer–polymer and polymer–particle interactions has to be balanced to avoid clustering of the particles in SMP-MNPC. For uniform heating in an AMF, a precise spatial and orientational positioning of the MNP within the polymer matrix is obligatory.[72] Although there have been several demonstrations of magnetic heating of SMP, the remote heating of the SMP-MNPC in physiological environments remains a challenge. The effects of the surrounding environment on the heat transport efficiency of the device need to be explored in detail. In addition, investigations regarding the biocompatibility of MNPC and the successful realization of clinical studies are also required. The unique combination of magnetically susceptible MNP and thermosensitive SMP will undoubtedly have additional applications and will continue to be actively researched in the coming years.

Abbreviations and symbols

AMF	alternating magnetic field
CMME	cyclic magneto-mechanical experiments
cPEVA	crosslinked poly[ethylene-*ran*-(vinyl acetate)]
DMTA	dynamic mechanical thermal analysis
DSCP	dual-shape creation procedure
DSE	dual-shape effect
DSP	dual-shape polymers
ΔT_g	temperature range of the glass transition process
ΔT_m	melting temperature range
ε	strain
ε_m	applied elongation in cyclic, thermomechanical tensile tests
f	frequency of AMF
H	magnetic field strength
H_c	coercivity
H_{def}	magnetic field strength used to deform the samples
H_{sw}	switching magnetic field strength
$H_{\sigma,max}$	magnetic field strength at stress maximum
MME	magnetic-memory effect
mNP	magnetic nanoparticles
MNP	magnetite nanoparticles
MNPC	magnetite nanoparticle composites
MSP	multiple-shape polymers

PEG	poly(ethylene glycol)
PEGMA	poly(ethylene glycol)monomethyl ether monomethacrylate
PEU	polyetherurethane
PCHMA	poly(cyclohexylmethacrylate)
PCL	poly(ε-caprolactone)
PCLDIMA	poly(ε-caprolactone) diisocyanatoethyldimethacrylate
R_r	shape-recovery ratio
R_f	shape-fixity ratio
M_r	remnant magnetization at $H = 0$
M_S	saturation magnetic limit
σ	stress
σ_{max}	maximum recovery stress
SME	shape-memory effect
SMP	shape-memory polymer
SMP-MNPC	shape-memory polymer magnetite nanoparticle composites
SMPU	shape-memory polyurethane
SNP	silica coated iron oxide nanoparticles
SPNP	superparamagnetic nanoparticles
S/V	surface area to volume ratio
TCP	triple-shape creation procedure
TMCP	temperature-memory creation procedure
TME	temperature-memory effect
TM-MNPC	temperature-memory MNPC
TMP	temperature-memory polymers
TMPU	temperature-memory polyurethane
TSP	triple-shape polymers
T_C	Curie temperature
T_{env}	environmental temperature
T_g	glass transition temperature
T_m	melting temperature
T_{max}	maximum achievable temperature
$T_{g,mix}$	glass transition temperature of the mixed phase
T_{perm}	highest thermal transition
T_{prog}	programming temperature in cyclic, thermomechanical tensile tests
T_{sw}	switching temperature
$T_{sw,bulk}$	bulk switching temperature
$T_{sw,app}$	apparent switching temperature
$T_{\sigma,max}$	temperature at which maximum recovery stress is observed
T_{trans}	transition temperature
wt%	weight percentage

References

1 M. Behl and A. Lendlein, *J. Mater. Chem.*, 2010, **20**, 3335–3345.
2 C. Liu, H. Qin and P. T. Mather, *J. Mater. Chem.*, 2007, **17**, 1543–1558.
3 P. T. Mather, X. F. Luo and I. A. Rousseau, *Annu. Rev. Mater. Res.*, 2009, **39**, 445–471.
4 D. Ratna and J. Karger-Kocsis, *J. Mater. Sci.*, 2008, **43**, 254–269.
5 J. Leng, X. Lan, Y. Liu and S. Du, *Prog. Mater. Sci.*, 2011, **56**, 1077–1135.
6 M. Behl, J. Zotzmann and A. Lendlein, *Adv. Polym. Sci.*, 2010, **226**, 1–40.
7 T. Xie, *Polymer*, 2011, **52**, 4985–5000.
8 L. Sun, W. M. Huang, C. C. Wang, Y. Zhao, Z. Ding and H. Purnawali, *J. Polym. Sci., Part A: Polym. Chem.*, 2011, **49**, 3574–3581.
9 A. Lendlein, M. Behl, B. Hiebl and C. Wischke, *Expert Rev. Med. Devices*, 2010, **7**, 357–379.
10 C. Wischke, A. T. Neffe, S. Steuer and A. Lendlein, *J. Controlled Release*, 2009, **138**, 243–250.
11 A. Lendlein and R. Langer, *Science*, 2002, **296**, 1673–1676.
12 Q. H. Meng and J. L. Hu, *Composites, Part A*, 2009, **40**, 1661–1672.
13 I. S. Gunes and S. C. Jana, *J. Nanosci. Nanotechnol.*, 2008, **8**, 1616–1637.
14 M. Behl and A. Lendlein, *Mater. Today*, 2007, **10**, 20–28.
15 I. Bellin, S. Kelch, R. Langer and A. Lendlein, *Proc. Natl. Acad. Sci. U. S. A.*, 2006, **103**, 18043–18047.
16 I. Bellin, S. Kelch and A. Lendlein, *J. Mater. Chem.*, 2007, **17**, 2885–2891.
17 T. Xie, X. C. Xiao and Y. T. Cheng, *Macromol. Rapid Commun.*, 2009, **30**, 1823–1827.
18 T. Ware, K. Hearon, A. Lonnecker, K. L. Wooley, D. J. Maitland and W. Voit, *Macromolecules*, 2012, **45**, 1062–1069.
19 C. Y. Bae, J. H. Park, E. Y. Kim, Y. S. Kang and B. K. Kim, *J. Mater. Chem.*, 2011, **21**, 11288–11295.
20 M. Behl, I. Bellin, S. Kelch, W. Wagermaier and A. Lendlein, *Adv. Funct. Mater.*, 2009, **19**, 102–108.
21 X. F. Luo and P. T. Mather, *Adv. Funct. Mater.*, 2010, **20**, 2649–2656.
22 T. Pretsch, *Smart Mater. Struct.*, 2010, **19**, 015006.
23 J. Zotzmann, M. Behl, Y. Feng and A. Lendlein, *Adv. Funct. Mater.*, 2010, **20**, 3583–3594.
24 S. J. Chen, J. L. Hu, C. W. M. Yuen, L. K. Chan and H. T. Zhuo, *Polym. Adv. Technol.*, 2010, **21**, 377–380.
25 J. Cui, K. Kratz, M. Heuchel, B. Hiebl and A. Lendlein, *Polym. Adv. Technol.*, 2010, **22**, 180–189.
26 M. Heuchel, J. Cui, K. Kratz, H. Kosmella and A. Lendlein, *Polymer*, 2010, **51**, 6212–6218.
27 J. Cui, K. Kratz and A. Lendlein, *Smart Mater. Struct.*, 2010, **19**, 065019–065029.
28 P. Miaudet, A. Derre, M. Maugey, C. Zakri, P. M. Piccione, R. Inoubli and P. Poulin, *Science*, 2007, **318**, 1294–1296.
29 K. Kratz, S. A. Madbouly, W. Wagermaier and A. Lendlein, *Adv. Mater.*, 2011, **23**, 4058–4062.
30 T. Xie, K. A. Page and S. A. Eastman, *Adv. Funct. Mater.*, 2011, **21**, 2057–2066.
31 L. Sun and W. M. Huang, *Soft Matter*, 2010, **6**, 4403–4406.
32 H. B. Lv, J. S. Leng, Y. J. Liu and S. Y. Du, *Adv. Eng. Mater.*, 2008, **10**, 592–595.
33 H. Y. Du and J. H. Zhang, *Soft Matter*, 2010, **6**, 3370–3376.
34 B. Yang, W. M. Huang, C. Li and L. Li, *Polymer*, 2006, **47**, 1348–1356.
35 W. M. Huang, B. Yang, L. An, C. Li and Y. S. Chan, *Appl. Phys. Lett.*, 2005, **86**, 114105–114108.
36 S. A. Madbouly and A. Lendlein, *Adv. Polym. Sci.*, 2010, **226**, 41–95.
37 G. Vialle, M. Di Prima, E. Hocking, K. Gall, H. Garmestani, T. Sanderson and S. C. Arzberger, *Smart Mater. Struct.*, 2009, **18**, 115014–115024.
38 D. J. Maitland, M. F. Metzger, D. Schumann, A. Lee and T. S. Wilson, *Lasers Surg. Med.*, 2002, **30**, 1–11.
39 W. Small, T. S. Wilson, W. J. Benett, J. M. Loge and D. J. Maitland, *Opt. Express*, 2005, **13**, 8204–8213.
40 C. M. Yakacki, N. S. Satarkar, K. Gall, R. Likos and J. Z. Hilt, *J. Appl. Polym. Sci.*, 2009, **112**, 3166–3176.
41 T. Gong, W. B. Li, H. M. Chen, L. Wang, S. J. Shao and S. B. Zhou, *Acta Biomater.*, 2012, **8**, 1248–1259.
42 X. J. Yu, S. B. Zhou, X. T. Zheng, T. Guo, Y. Xiao and B. T. Song, *Nanotechnology*, 2009, **20**, 235702.
43 P. E. Le Renard, R. Lortz, C. Senatore, J. P. Rapin, F. Buchegger, A. Petri-Fink, H. Hofmann, E. Doelker and O. Jordan, *J. Magn. Magn. Mater.*, 2011, **323**, 1054–1063.
44 M. P. Marszall, *Pharm. Res.*, 2011, **28**, 480–483.
45 F. Fahrni, M. W. J. Prins and L. J. van Ijzendoorn, *J. Magn. Magn. Mater.*, 2009, **321**, 1843–1850.
46 L. L. Lao and R. V. Ramanujan, *J. Mater. Sci.: Mater. Med.*, 2004, **15**, 1061–1064.

47 P. R. Buckley, G. H. McKinley, T. S. Wilson, W. Small, W. J. Benett, J. P. Bearinger, M. W. McElfresh and D. J. Maitland, *IEEE Trans. Biomed. Eng.*, 2006, **53**, 2075–2083.
48 R. Mohr, K. Kratz, T. Weigel, M. Lucka-Gabor, M. Moneke and A. Lendlein, *Proc. Natl. Acad. Sci. U. S. A.*, 2006, **103**, 3540–3545.
49 Y. C. Jung, H. H. Kim, Y. A. Kim, J. H. Kim, J. W. Cho, M. Endo and M. S. Dresselhaus, *Macromolecules*, 2010, **43**, 6106–6112.
50 J. S. Leng, W. M. Huang, X. Lan, Y. J. Liu and S. Y. Du, *Appl. Phys. Lett.*, 2008, **92**, 204101–204103.
51 H. Koerner, J. Kelley, J. George, L. Drummy, P. Mirau, N. S. Bell, J. W. P. Hsu and R. A. Vaia, *Macromolecules*, 2009, **42**, 8933–8942.
52 T. Hanemann and D. V. Szabo, *Materials*, 2010, **3**, 3468–3517.
53 K. Babiuch, R. Wyrwa, K. Wagner, T. Seemann, S. Hoeppener, C. R. Becer, R. Linke, M. Gottschaldt, J. Weisser, M. Schnabelrauch and U. S. Schubert, *Biomacromolecules*, 2011, **12**, 681–691.
54 S. Wada, K. Tazawa, I. Furuta and H. Nagae, *Oral Dis.*, 2003, **9**, 218–223.
55 F. Dong, W. Guo, J.-H. Bae, S.-H. Kim and C.-S. Ha, *Chem.–Eur. J.*, 2011, **17**, 12802–12808.
56 L. Xiao, J. Li, D. F. Brougham, E. K. Fox, N. Feliu, A. Bushmelev, A. Schmidt, N. Mertens, F. Kiessling, M. Valldor, B. Fadeel and S. Mathur, *ACS Nano*, 2011, **5**, 6315–6324.
57 C. H. Li, P. Hodgins and G. P. Peterson, *J. Appl. Phys.*, 2011, **110**, 054303.
58 H. Kobayashi, K. Ueda, A. Tomitaka, T. Yamada and Y. Takemura, *IEEE Trans. Magn.*, 2011, **47**, 4151–4154.
59 Y. Xu, D.-l. Zhao, L.-y. Zhao and J.-t. Tang, *FMA 2010 E-Book*, 2010, pp. 197–201.
60 D. L. LesliePelecky and R. D. Rieke, *Chem. Mater.*, 1996, **8**, 1770–1783.
61 T. Weigel, R. Mohr and A. Lendlein, *Smart Mater. Struct.*, 2009, **18**, 025011.
62 M. Y. Razzaq, M. Anhalt, L. Frormann and B. Weidenfeller, *Mater. Sci. Eng., A*, 2007, **444**, 227–235.
63 M. Y. Razzaq, M. Behl, K. Kratz and A. Lendlein, *Mater. Res. Soc. Symp. Proc.*, 2009, **1140**, 185–190.
64 U. N. Kumar, K. Kratz, W. Wagermaier, M. Behl and A. Lendlein, *J. Mater. Chem.*, 2010, **20**, 3404–3415.
65 U. N. Kumar, K. Kratz, M. Behl and A. Lendlein, *eXPRESS Polym. Lett.*, 2012, **6**, 26–40.
66 M. Behl, I. Bellin, S. Kelch, W. Wagermaier and A. Lendlein, *Mater. Res. Soc. Symp. Proc.*, 2009, **1140**, 3–8.
67 A. Lendlein, J. Zotzmann, Y. Feng, A. Alteheld and S. Kelch, *Biomacromolecules*, 2009, **10**, 975–982.
68 U. N. Kumar, K. Kratz, M. Heuchel, M. Behl and A. Lendlein, *Adv. Mater.*, 2011, **23**, 4157–4162.
69 M. Y. Razzaq, M. Behl and A. Lendlein, *Adv. Funct. Mater.*, 2012, **22**, 184–191.
70 J. Gass, P. Poddar, J. Almand, S. Srinath and H. Srikanth, *Adv. Funct. Mater.*, 2006, **16**, 71–75.
71 Y. Haldorai, V. H. Nguyen, Q. L. Pham and J.-J. Shim, *Composite Interfaces*, 2012, **18**, 259–274.
72 P. Schexnailder and G. Schmidt, *Colloid Polym. Sci.*, 2009, **287**, 1–11.